Cloud Detection over the Arctic Region Using Airborne Imaging Spectrometer Data during the Daytime

BO-CAI GAO

Remote Sensing Division, Naval Research Laboratory, Washington, D.C.

WEI HAN

SFA, Inc., Largo, Maryland

SI CHEE TSAY

Climate and Radiation Branch, NASA/Goddard Space Flight Center, Greenbelt, Maryland

NORTH F. LARSEN

Geophysical Institute and Department of Physics, University of Alaska, Fairbanks, Alaska

(Manuscript received 29 September 1997, in final form 19 February 1998)

ABSTRACT

Detection of clouds over arctic regions from current satellite radiometric measurements in the visible and IR atmospheric window regions, such as those of Advanced Very High Resolution Radiometer and Landsat, is often difficult due to the high albedos of snow- and ice-covered surfaces in the visible and the nearly isothermal temperature profiles in the lower atmosphere. In this paper the authors show that the water vapor absorption channel at 1.38 μm is effective in detecting high clouds over snow- and ice-covered surfaces in the Arctic. Low-level clouds can be detected from surface snow and sea ice using a narrow channel centered at 1.5 μm with a width of approximately 10 nm because of the dark background that results from strong absorption by snow and sea ice. Imaging data with contiguous spectral coverage between 0.4 and 2.5 μm acquired with the Airborne Visible/Infrared Imaging Spectrometer during the Arctic Radiation Measurements in Column Atmosphere-Surface System in Alaska in 1995 are analyzed. The authors have observed that as wavelength increases from 1.38 μm the atmospheric water vapor absorption becomes weaker and weaker and the low-level clouds and surface tundra are increasingly seen. It is always possible to locate a narrow channel in the spectral range of 1.38–1.50 μm with appropriate water vapor absorption strength to separate water and ice clouds from surface snow, sea ice, and tundra. The simple cloud-masking technique described here is directly applicable to cloud detection during the daytime from hyperspectral imaging data over arctic regions, which will be acquired with future satellite sensors.

1. Introduction

Cloud detection from remote sensing data continues to be an area of active research (see, for example, Li and Leighton 1991; Ebert 1987, 1989, 1992; Key and Barry 1989; Key 1990; Welch et al. 1990, 1992, 1996). In the visible and thermal window regions, threshold tests are the primary technique currently employed in cloud detection algorithms. An example of such techniques is that pixels with visible reflectances 3% higher than the surrounding background pixels and with brightness temperatures 3°C below the background pixels are identified as cloudy (Welch et al. 1996). However, threshold methods have experienced difficulties in the arctic regions stemming from low to no contrast between clouds and underlying snow–sea ice surface in the visible reflectances and the IR brightness temperatures (Rossow et al. 1989; Stowe et al. 1989). An additional difficulty in the arctic regions is created by temperature inversions, which may cause clouds to appear to be even warmer than the underlying snow or ice surfaces. To illustrate these cloud detection difficulties, examples of Moderate Resolution Imaging Spectrometer (MODIS) Airborne Simulator (MAS) (King et al. 1996) radiance images for two channels centered at 0.66 and 11 μm are presented in Figs. 1a and 1b, respectively. These images were acquired over the North Slope region of Alaska during the Arctic Radiation Measurements in

Corresponding author address: Dr. Bo-Cai Gao, Naval Research Laboratory, Remote Sensing Division, Code 7212, 4555 Overlook Drive, SW, Washington, DC 20375.
E-mail: gao@neptune.nrl.navy.mil

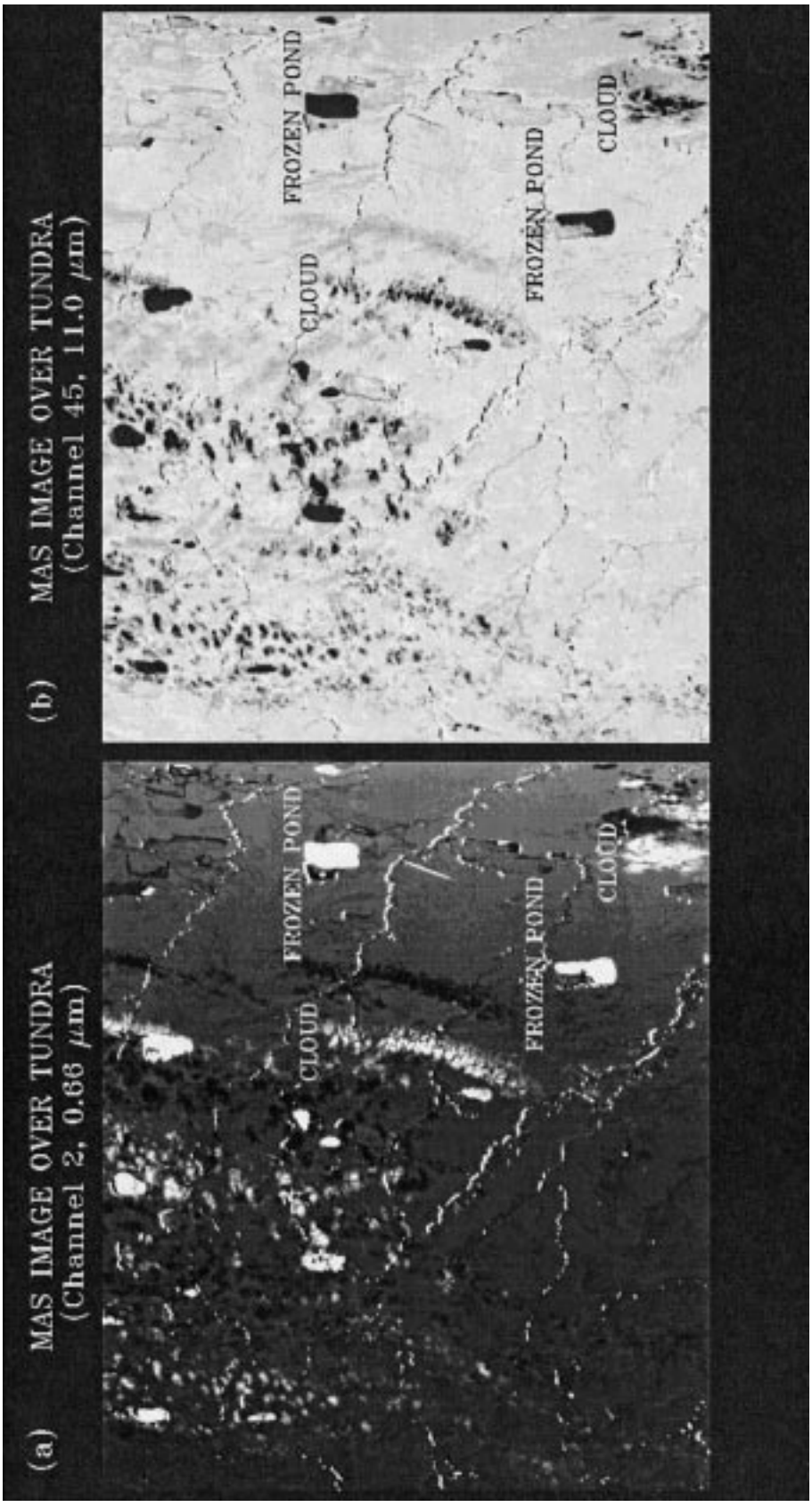

FIG. 1. MAS radiance images over the northern foothills of the Brook Range on 13 June 1995: (a) 0.66 and (b) 11.0 μm.

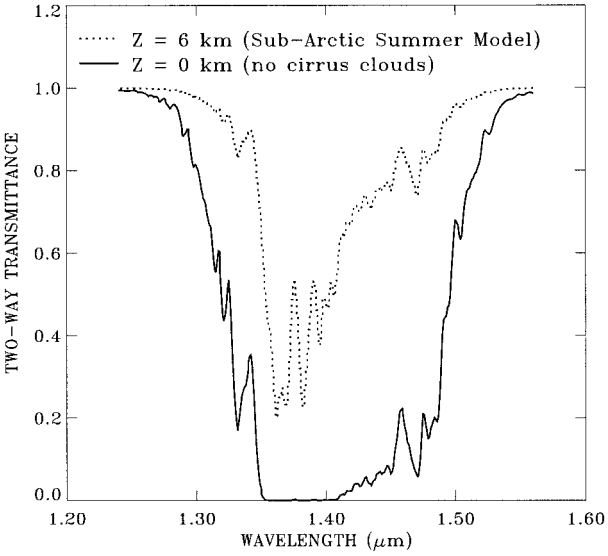

FIG. 2. Two-way path, clear-sky transmittance spectra for the subarctic summer atmospheric model (2.1 cm of precipitable water). The incoming segment of the path has a 45° zenith angle and ends at altitude *Z* (where 100% reflection is assumed). The outgoing segment has a 0° zenith angle. The *Z*'s are chosen at 0 and 6 km.

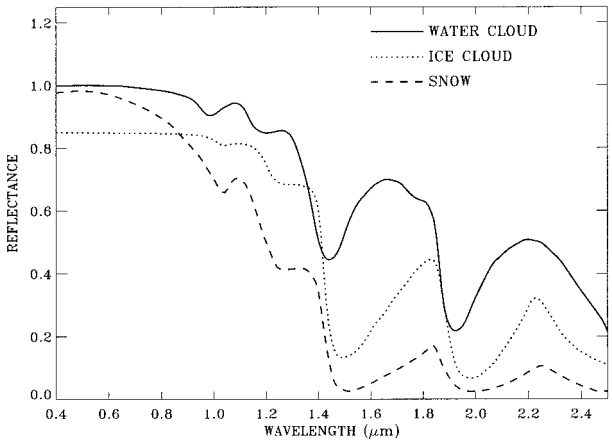

FIG. 3. Simulated directional–hemispherical reflectance spectra of a water cloud, an ice cloud, and a snow surface at an illumination angle of 60°, for wavelengths from 0.4 to 2.5 μm (Dozier 1989). Cloud liquid water equivalences are 10 mm for the water cloud and 1 mm for the ice cloud. The radii of the water droplets and ice crystals are 10 and 40 μm, respectively. The snow is assumed to be infinitely deep, with grain radii of 200 μm. The simulations were made using a two-stream radiative transfer code.

Column Atmosphere-Surface System (ARMCAS) field campaign in June 1995. In the 0.66-μm visible image (Fig. 1a), both clouds, apparent from the shadows that they cast, and frozen ponds appear bright because their reflectances are higher than those of the surrounding arctic tundra. The 11-μm IR image in Fig. 1b displays that clouds and frozen ponds both appear to be very dark due to their cold temperatures. Using traditional threshold techniques it is almost impossible in such images to discriminate clouds from frozen ponds.

In the past, many cloud detection algorithms were developed based on the analysis of existing data measured with current satellite instruments having only a few discrete channels [e.g., the Advanced Very High Resolution Radiometer (AVHRR)]. There has been relatively little work done on imaging spectrometer data with contiguous spectral coverage. Based on observations from spectral imaging data acquired with the Airborne Visible Infrared Imaging Spectrometer (AVIRIS) (Vane et al. 1993) flying on an ER-2 aircraft at 20-km altitude, Gao et al. (1993) have reported that near-IR channels close to the centers of the 1.38- and 1.88-μm water vapor bands are very useful for detecting thin cirrus clouds. However, under dry atmospheric conditions, these channels may also detect lower-level clouds and underlying surfaces because total absorption of solar radiation by water vapor on the sun–surface–sensor path in these channels may not occur. Concerns have been raised about the capability of detecting thin cirrus under dry atmospheric conditions with the 1.38-μm channel (Ben-Dor 1994; Hutchison and Choe 1996).

Imaging spectrometer data over the arctic regions were first acquired in June 1995 during the ARMCAS campaign. In this paper, we demonstrate that the 1.38-μm channel is still very effective for detecting clouds over snow and ice surfaces in the dry arctic regions. We also demonstrate that imaging spectrometer data with contiguous spectral coverage between 1.38 and 1.5 μm makes cloud detection over arctic regions during the daytime simpler than with current satellite data since these satellites have only a few discrete channels.

2. The experimental data

The ARMCAS field campaign was deployed in the Arctic tundra region surrounding Prudhoe Bay, Alaska, and the snow- and ice-covered Beaufort Sea during 1–15 June 1995. The main goal of this experiment was to improve our understanding of the mechanisms in cloud microphysics, radiation, and remote sensing in the Arctic. The experiment includes satellite remote sensing (AVHRR), high-altitude remote sensing [National Aeronautic and Space Administration's (NASA) ER-2 aircraft at 20 km], boundary layer in situ measurements (University of Washington's C-131A aircraft), radiosondes, and ground-based measurements (Tsay et al. 1995).

One of the instruments on board the NASA ER-2 aircraft was AVIRIS. It is an imaging spectrometer that measures reflected solar radiation in a spectral range from 0.4 to 2.5 μm with 224 narrow and contiguous channels that have widths of approximately 10 nm. From a nominal ER-2 altitude of 20 km, AVIRIS has a ground instantaneous field of view of 20 m $\times$ 20 m and a 10.5-km swath width. It has reliable geometrical, radiometric, and spectral calibrations (Green et al. 1993). During ARMCAS, AVIRIS collected more than 40 gi-

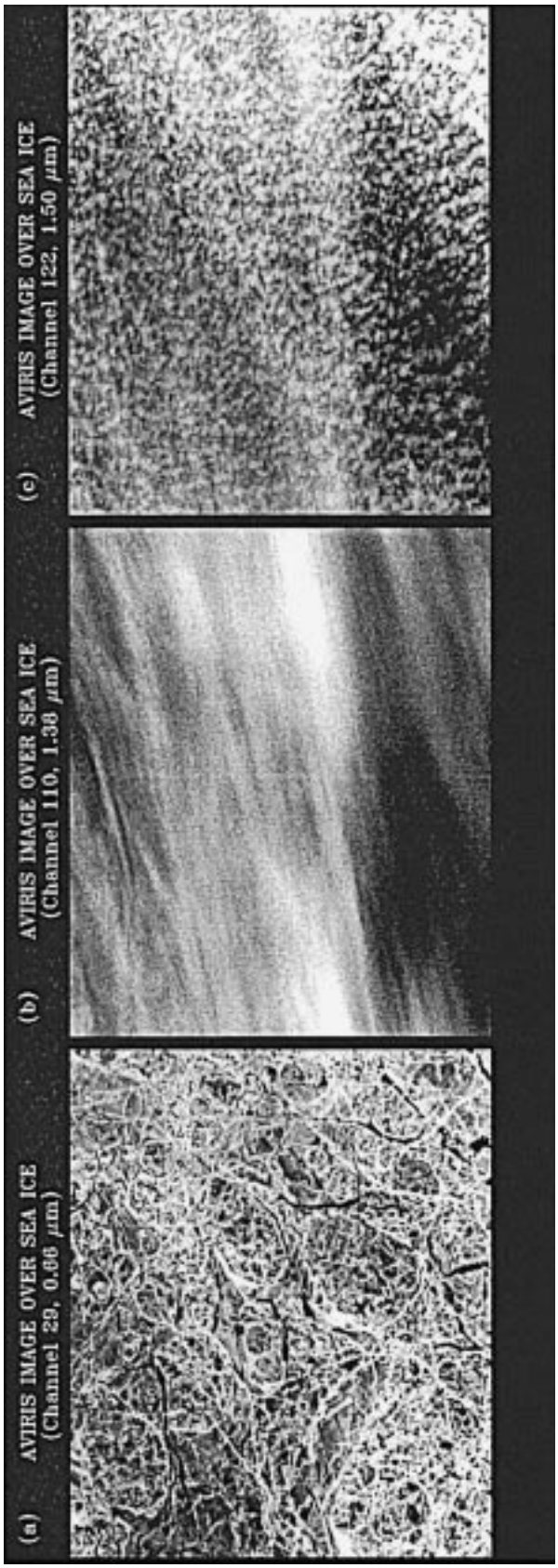

FIG. 4. AVIRIS image over Prudhoe Bay, Alaska, on 11 June 1995: (a) 0.66 μm, showing sea ice; (b) 1.38 μm, showing only the cirrus clouds; and (c) 1.50 μm, showing low-level clouds and cirrus clouds.

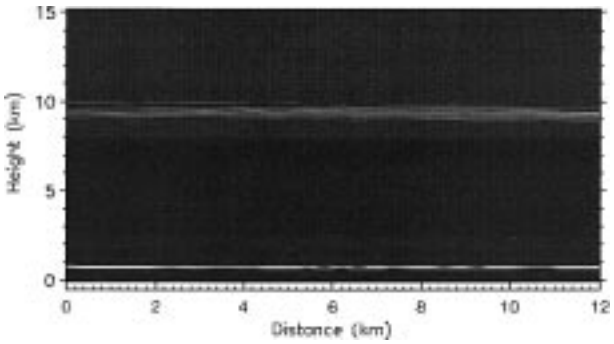

FIG. 5. CLS measurements taken over a transect corresponding to a vertical line in the center of Fig. 4. High clouds (cirrus) and low-level clouds are shown.

gabytes of data over areas covered by green tundra; refrozen ponds; dark, open ocean; bright snow; and sea ice. Also on board the ER-2 aircraft were MAS and a cloud lidar system (CLS). The MAS is an imaging spectrometer measuring reflected solar and emitted thermal radiation in 50 narrow spectral channels between 0.55 and 14.2 μm (King et al. 1996). The CLS is a nadir-pointing lidar that provides heights and density profiles of clouds (Spinhirne et al. 1982).

3. Cloud detection over snow and sea ice

Clouds located above approximately 6 km in the arctic region are often composed of ice crystals (Liou 1992). Typically about 90%–99% of the atmospheric water vapor is distributed in the lower atmosphere below cirrus clouds. Under clear atmospheric conditions, AVIRIS channels located near the center of the strong 1.38-μm water vapor band receive little radiance reflected from low-level clouds and underlying surfaces because the solar radiation is almost completely absorbed by water vapor in its path. However, in the presence of cirrus clouds, the radiance near 1.38 μm measured by the AVIRIS sensor is much larger because cirrus clouds are located at higher altitudes and the solar radiation scattered by cirrus clouds can reach the AVIRIS instrument. To illustrate how strongly the solar radiation in the 1.38-μm water vapor band absorption region is attenuated in the atmosphere, we computed two-way, clear-sky transmittance from the sun to a given level Z in the atmosphere and from level Z to the top of the atmosphere using the LOWTRAN-7 program (Kneizys et al. 1988). The computations shown are for a nadir-viewing geometry and a 45° solar zenith angle. Figure 2 illustrates the two-way transmittance in the 1.24–1.56-μm spectral region for altitudes of 0 and 6 km and for the subarctic summer model atmosphere. From the $Z = 0$ km spectrum, the two-way transmittance at 1.38 μm is close to zero, and total absorption of solar radiation has occurred. From the $Z = 6$ km spectrum, it is seen clearly that as the wavelength increases from 1.38 to 1.50 μm, the atmospheric water vapor absorption decreases significantly. The absorption is less than 5% at 1.50 μm.

Low-level clouds are usually composed of water droplets. They may be discerned from background snow or sea ice, which possesses absorption properties that differ from those of liquid water in the near-IR spectral region. Figure 3 shows examples of simulated directional–hemispherical reflectance spectra of a water cloud, an ice cloud, and a snow surface (Dozier 1989). The snow surface has strong ice absorption bands centered near 1.50 and 2.0 μm, a region in which water clouds have weak absorption and ice clouds have medium absorption. Snow and sea ice can appear much darker than water clouds in the 1.5- and 2.0-μm images. This allows the discerning of water clouds from snow- or sea-ice-covered clear surfaces.

An example of detection of both the upper-level thin cirrus and the lower-level water clouds is presented in Figs. 4a–c, which display AVIRIS images for channels centered at 0.66, 1.38, and 1.50 μm, respectively. These images were taken over an area centered approximately at 72.8°N, 151.0°W near Prudhoe Bay, Alaska, during ARMCAS on 11 June 1995. The 0.66-μm image appears to be cloud free with complex spatial patterns of sea ice. However, the 1.38-μm image shows that the upper-level thin cirrus clouds are present over most of the scene. There are no sea-ice spatial patterns or cumulus clouds discernible from this image. The 1.50-μm image depicts the upper-level cirrus and the lower-level cumulus clouds. Background sea ice looks dark in the 1.50-μm image because sea ice on the surface has strong absorption. The two-layer cloud structure apparent in this scene is also detected by simultaneous CLS measurements, as shown in Fig. 5. Cirrus clouds are seen above 5 km, and very low clouds are apparent within 1 km above ground. The images in Fig. 4 illustrate that the 1.38-μm channel is very useful in detecting thin cirrus clouds from sea ice under the dry arctic atmospheric conditions and that low-level clouds can also be separated from background sea ice with the 1.50-μm AVIRIS channel.

Another example of detecting water clouds over snow- and sea-ice-covered surfaces is illustrated in Fig. 6. A 0.66-μm AVIRIS image at 70.5°N, 147.0°W, acquired over Prudhoe Bay during ARMCAS on 4 June 1995, is shown in Fig. 6a. Parts of the surface areas covered by sea ice are brighter than clouds, and the discrimination of clouds from sea-ice-covered regions is difficult. The 1.38-μm image (not shown here) over this scene is dark with maximum reflectance values less than 0.008, which indicates that there are no cirrus clouds in the scene. Figure 6b shows the 1.50-μm AVIRIS image over the same region. Extensive cumulus clouds are noted in many parts of the scene. Bare sea ice is dark in this image because of the strong absorption of ice particles in the 1.50-μm spectral region. Fresh snow with fine ice particles, which absorb less solar energy than larger sea ice particles, appears slightly

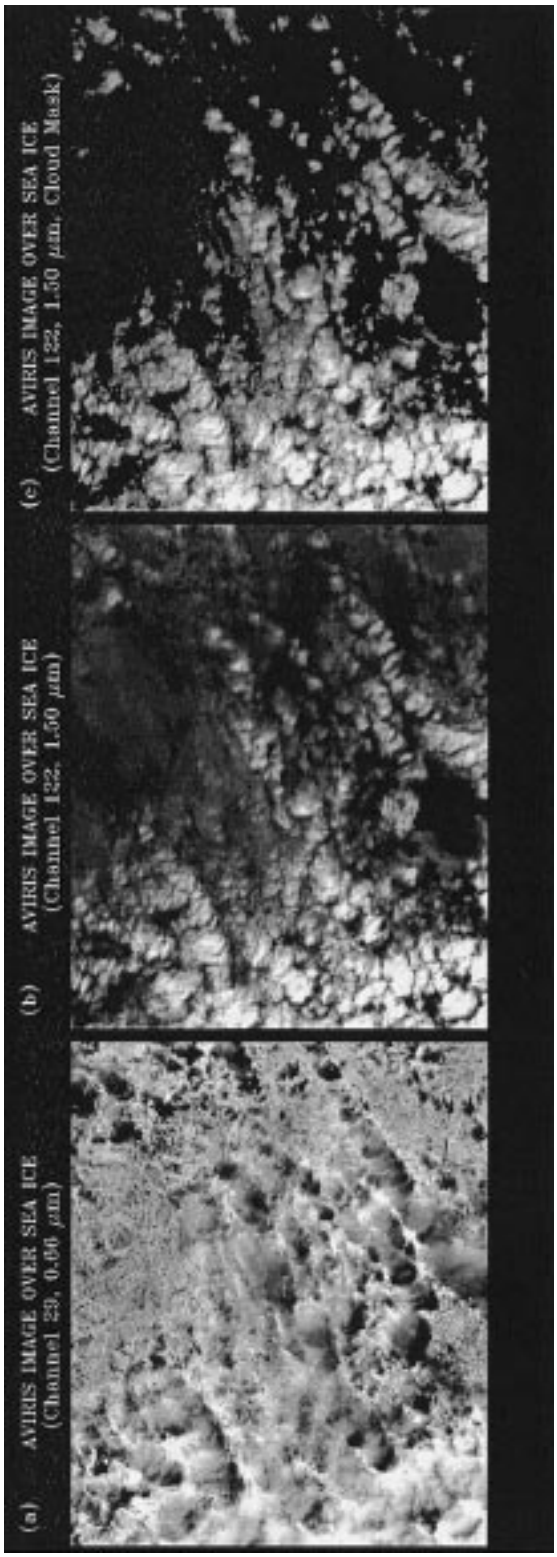

FIG. 6. AVIRIS image over Prudhoe Bay, Alaska, on 4 June 1995: (a) 0.66 and (b) 1.50 μm. (c) An image processed by the threshold method to the 1.50-μm image. It shows low-level clouds only.

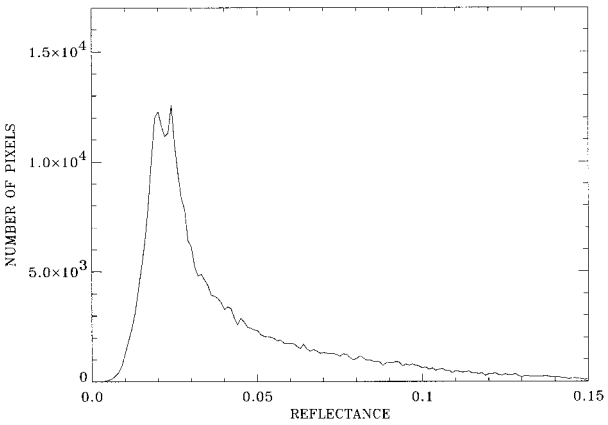

FIG. 7. Histogram of the 1.50-μm reflectance, as shown in Fig. 6b.

brighter than clear sea ice. Figure 7 shows the histogram of the 1.50-μm image (in reflectance units). Clear pixels are distributed in the lower end of the histogram and peak occurs at a reflectance value of about 0.02, while the cloudy pixels are distributed in the upper end, the long tail portion, of the histogram. Assuming the apparent reflectance values of clear pixels following a Gaussian distribution and with careful visual examination of the shape of the histogram, we can select a threshold value of 0.035. Pixels with reflectance values greater than this threshold are considered to be cloudy. The resulting cloud mask of this image is shown in Fig. 6c. In this image cumulus clouds are clearly seen and the features of surface sea ice and snow disappear. In this example, cumulus clouds are separated from background snow and sea ice using an AVIRIS channel centered at 1.50 μm—the peak position of an ice absorption band.

4. Cloud detection over tundra

The reflectance of arctic tundra in the 1.5–2.5-μm spectral region can be comparable to, and in some cases greater than, the reflectance of water clouds, unlike snow and sea ice that are usually darker than water clouds in this spectral region. To separate clouds from tundra, we use narrow AVIRIS channels located in the 1.38–1.50-μm wavelength interval. We have observed from AVIRIS data that a narrow channel located at the center of the strong 1.38-μm water vapor absorption band can see both the upper-level cirrus clouds and the lower-lever water clouds over tundra under dry atmospheric conditions. The surface tundra makes little contribution to radiance measured at this channel. As wavelength increases from 1.38 to 1.50 μm, water vapor absorption decreases significantly (see Fig. 2), and low-level water clouds and surface features are increasingly seen. It is always possible to locate a channel in the spectral range of 1.38–1.50 μm with appropriate water vapor absorption strength in which both the thin, cirrus clouds and the lower-level cumulus clouds are seen, but the surface features are eliminated due to additional absorption of solar radiation by water vapor between clouds and surface areas.

Figure 8 shows AVIRIS images at 69.5°N, 148.5°W, acquired in the northern foothills of the Brooks Range of Alaska during ARMCAS on 7 June 1995. Cumulus clouds are seen in the 0.66-μm image (Fig. 8a). A small thin cirrus cloud is apparent in the upper-right corner. Also shown in Fig. 8a are surface features, such as frozen ponds, a road, and snow-covered areas. The 1.38-μm image (Fig. 8b) shows thin, cirrus clouds and part of a large cumulus cloud. Thin low-level clouds and surface features are not visible in this image. The 1.42- and 1.43-μm images, adjacent channels, are shown in Figs. 8c and 8d, respectively. These channels are located off the center of the strong 1.38-μm water vapor absorption band; thus, the water vapor absorption is weaker than the absorption at the 1.38-μm channel (see Fig. 2). This explains why more clouds appear in the 1.42-μm image than in the 1.38-μm image. As the wavelength increases by one more channel toward longer wavelengths, some surface features reappear in the 1.43-μm image because the water vapor absorption is reduced slightly more in the 1.43-μm channel than in the 1.42-μm channel. Therefore, the AVIRIS channel centered at 1.42 μm has appropriate water vapor absorption strength for detecting clouds (including cirrus and lower-level clouds) from tundra. Because the amount of water vapor in the atmosphere can vary and the strength of water vapor absorption varies significantly between 1.38 and 1.50 μm, from total absorption at 1.38 μm to nearly total transparent at 1.50 μm, one is able to locate an appropriate narrow channel in the spectral range of 1.38–1.50 μm to separate clouds from tundra for a given atmospheric condition.

5. Discussion

We tested several techniques for detecting clouds using only narrow channels (approximately 10 nm wide) located in atmospheric window regions, such as those centered near 0.66, 0.86, 1.64, and 2.2 μm. For example, we tried to use the ratio image of the 1.64-μm channel over the 0.86-μm channel in conjunction with a threshold method for separating clouds from snow- and sea-ice-covered surfaces. A similar ratio technique was previously used for cloud detections from data acquired through the Defense Meteorological Satellite Program (Bunting and d'Entremont 1982). We found that the ratio image allowed the detection of thick clouds but failed to detect partially transparent thin clouds. We also tried to separate clouds from arctic tundra using the ratio image of the 0.86-μm channel over the 0.66-μm channel. The idea behind this ratio is that clouds have similar reflectance at both wavelengths, while tundra has smaller reflectance at 0.66 μm than at 0.86 μm because of strong chlorophyll absorption at 0.66 μm. The ratio val-

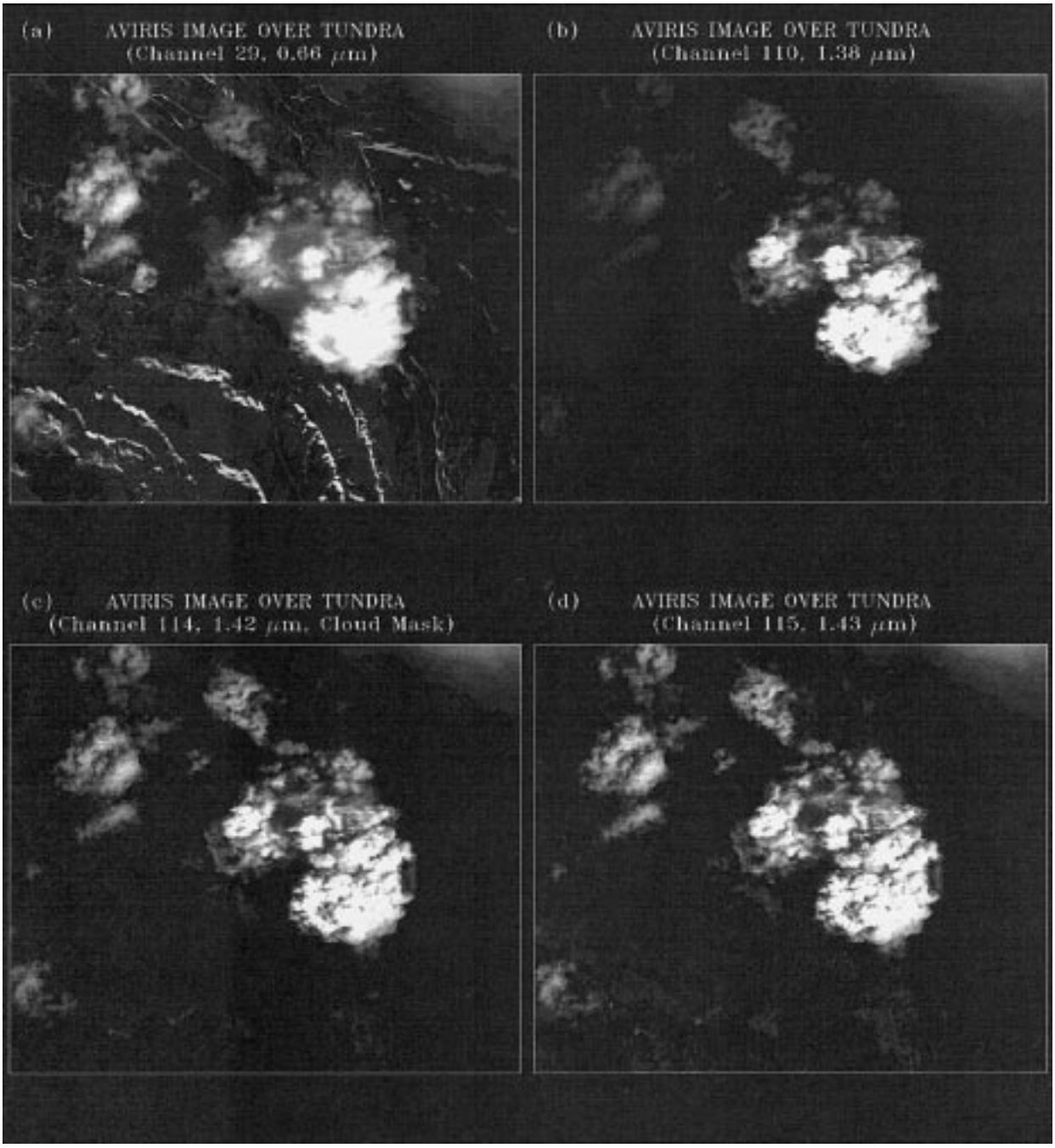

FIG. 8. AVIRIS image over the northern foothills of the Brook Range of Alaska on 7 June 1995: (a) 0.66, (b) 1.38, (c) 1.42, and (d) 1.43 μm.

ues should be close to 1 for thick clouds and much greater than 1 for clear tundra pixels. Again, the ratio image allowed the detection of thick clouds but failed to detect thin clouds.

The strengths of water vapor absorption in the 1.8–2.0-μm spectral region, similar to those in the 1.38–1.5-μm region, also vary significantly. In principle, it is possible to locate an appropriate narrow channel in this spectral range to separate clouds from clear-surface areas. However, because the solar energy in the 1.88–2.0-μm region is only approximately 40% of that in the 1.38–1.50-μm region and because enhanced cloud absorption by liquid water and ice occurs in the 1.88–2.0-μm region, the signal-to-noise ratios of AVIRIS images in the 1.88–2.0-μm region are significantly lower than those in the 1.38–1.50-μm region. Therefore, narrow

channels in the 1.38–1.50-μm region are used for cloud detection over arctic regions.

At present, hyperspectral imaging instruments covering the complete solar spectral region between 0.4 and 2.5 μm are being built for remote sensing of land, ocean, and atmosphere from future satellite platforms (e.g., Ungar 1997). The techniques described here using narrow channels within the 1.38-μm water vapor band absorption region to detect artic clouds are directly applicable to data from hyperspectral imagers on board future spacecrafts for cloud-masking purposes.

6. Summary

Based upon analysis of spectral imaging data acquired with AVIRIS from a NASA ER-2 aircraft over arctic regions, we have found that a 1.38-μm image is very useful for detecting high clouds during the daytime over the dry arctic environment. Because the strength of water vapor absorption from 1.38 to 1.50 μm decreases significantly (from total absorption to nearly no absorption), as the wavelength increases from 1.38 μm toward longer wavelengths, the low-level water clouds and surface features are increasingly seen. It is always possible to locate a narrow channel ($\sim$10 nm wide) in the spectral range of 1.38–1.50 μm with appropriate water vapor absorption strength in which both the thin cirrus clouds and the lower-level, cumulus clouds can be seen, but the surface features are eliminated due to additional absorption of solar radiation by water vapor between clouds and surface areas. We also found that lower-level water clouds can be separated from background snow and sea ice using a narrow channel located at the 1.50-μm ice absorption band center. In general, the use of narrow channels between 1.38 and 1.50 μm allows improved detection of thin water and ice clouds.

Acknowledgments. The authors are grateful to R. O. Green of the Jet Propulsion Laboratory for providing the AVIRIS data and to J. D. Spinhirne's research group of the NASA/Goddard Space Flight Center for providing CLS data. The acquisition of AVIRIS data during the ARMCAS campaign was supported by a grant from NASA Headquarters and the Office of Mission to Planet Earth.

REFERENCES

Ben-Dor, E., 1994: A precaution regarding cirrus cloud detection from airborne imaging spectrometer data using the 1.38-μm water vapor band. *Remote Sens. Environ.,* **50,** 346–350.

Bunting, J. T., and R. P. d'Entremont, 1982: Improved cloud detection utilizing defense meteorological satellite program near infrared measurements. AFGL-TR-82-0027, Air Force Geophysics Laboratory, Bedford, MA, 91 pp. [Available from Air Force Research Laboratory, Bedford, MA 01731.]

Dozier, J., 1989: Spectral signature of alpine snow cover from the Landsat Thematic Mapper. *Remote Sens. Environ.,* **28,** 9–22.

Ebert, E., 1987: A pattern recognition technique for distinguishing surface and cloud types in the polar regions. *J. Climate Appl. Meteor.,* **26,** 1412–1427.

——, 1989: Analysis of polar clouds from satellite imagery using pattern recognition and a statistical cloud analysis scheme. *J. Appl. Meteor.,* **28,** 382–399.

——, 1992: Pattern recognition analysis of polar clouds during summer and winter. *Int. J. Remote Sens.,* **13,** 97–109.

Gao, B.-C., A. F. H. Goetz, and W. J. Wiscombe, 1993: Cirrus cloud detection from airborne imaging spectrometer data using the 1.38-μm water vapor band. *Geophys. Res. Lett.,* **20,** 301–304.

Green, R. O., J. E. Conel, M. Helmlinger, J. Van den Bosch, C. Chovit, and T. Chrien, 1993: Inflight calibration of AVIRIS in 1992 and 1993. JPL Publ. 93-26, 1, Jet Propulsion Laboratory, Pasadena, CA, 69–72. [Available from Jet Propulsion Laboratory, 4800 Oak Grove Road, Pasadena, CA 91109.]

Hutchison, K. D., and N. J. Choe, 1996: Application of 1.38-μm imagery for thin cirrus detection in daytime imagery collected over land surfaces. *Int. J. Remote Sens.,* **17,** 3325–3342.

Key, J., 1990: Cloud cover analysis with arctic AVHRR data, Part II: Classification with spectral and textural measures. *J. Geophys. Res.,* **95,** 7661–7675.

——, and R. G. Barry, 1989: Cloud cover analysis with arctic AVHRR data, Part I: Cloud detection. *J. Geophys. Res.,* **94,** 18 521–18 535.

King, M. D., and Coauthors, 1996: Airborne scanning spectrometer for remote sensing of cloud, aerosol, water vapor, and surface properties. *J. Atmos. Oceanic Technol.,* **13,** 777–794.

Kneizys, F., E. Shettle, L. Abreu, J. Chetwynd, G. Anderson, W. Gallery, J. E. A. Selby, and S. Clough, 1988: User's guide to LOWTRAN-7. AFGL-TR-83-0187, Air Force Geophysics Laboratory, Bedford, MA, 137 pp. [Available from Air Force Research Laboratory, Bedford, MA 01731.]

Li, Z., and H. G. Leighton, 1991: Scene identification and its effect on cloud radiative forcing in the Arctic. *J. Geophys. Res.,* **96,** 9175–9188.

Liou, K. N., 1992: *Radiation and Cloud Processes in the Atmosphere.* Oxford University Press, 487 pp.

Rossow, W. B., C. L. Brest, and L. C. Garder, 1989: Global, seasonal surface variations from satellite radiance measurements. *J. Climate,* **2,** 214–247.

Spinhirne, J. D., M. Z. Hansen, and L. O. Caudill, 1982: Cloud top remote sensing by airborne lidar. *Appl. Opt.,* **22,** 1564–1571.

Stowe, L. L., H. Y. M. Yeh, T. F. Eck, C. G. Wellemeyer, H. L. Kyle, and the *Nimbus-7* Cloud Data Processing Team, 1989: *Nimbus-7* global cloud climatology. Part II: First year results. *J. Climate,* **2,** 671–709.

Tsay, S. C., M. D. King, and P. V. Hobbs, 1995: Arctic radiation measurements in column atmosphere–surface system—Science plan. NASA GSFC Internal Rep., 18 pp. [Available from NASA/Goddard Space Flight Center, Code 913, Greenbelt, MD 20771.]

Ungar, S. G., 1997: Technology for future Landsat missions. *Photogramm. Eng. Remote Sens.,* **63,** 901–905.

Vane, G., R. O. Green, T. G. Chrien, H. T. Enmark, E. G. Hansen, and W. M. Porter, 1993: The Airborne Visible/Infrared Imaging Spectrometer. *Remote Sens. Environ.,* **44,** 127–143.

Welch, R. M., K. S. Kuo, and S. K. Sengupta, 1990: Cloud and surface textural features in polar regions. *IEEE Trans. Geosci. Remote Sens.,* **28,** 520–528.

——, S. K. Sengupta, A. K. Goroch, P. Rabindra, N. Rangaraj, and M. S. Navar, 1992: Polar cloud and surface classification using AVHRR imagery: An intercomparison of methods. *J. Appl. Meteor.,* **31,** 405–420.

——, R. E. Feind, T. A. Berendes, D. E. Lloyd, and A. M. Logar, cited 1996: The ASTER polar cloud mask algorithm theoretical basis document. [Available online at http://eospso.gsfc.nasa.gov/atbd/astertables.html]